Journal of Power Sources 195 (2010) 2372–2376

Contents lists available at ScienceDirect

Journal of Power Sources

journal homepage: www.elsevier.com/locate/jpowsour

Short communication

Carbon-coated MoO_3 nanobelts as anode materials for lithium-ion batteries

M.F. Hassan[a,c,*], Z.P. Guo[a,b], Z. Chen[b], H.K. Liu[a]

[a] Institute for Superconducting and Electronic Materials, University of Wollongong, NSW 2522, Australia
[b] School of Mechanical, Mechatronic & Materials Engineering, University of Wollongong, NSW 2522, Australia
[c] Department of Science Physics, Faculty of Science and Technology, University of Malaysia Terengganu, Kuala Terengganu 21030, Malaysia

ARTICLE INFO

Article history:
Received 11 August 2009
Received in revised form 3 September 2009
Accepted 6 October 2009
Available online 30 October 2009

Keywords:
Molybdenum oxide
Hydrothermal method
Carbon coating
Anode materials
Lithium-ion batteries

ABSTRACT

MoO_3 nanobelts are synthesized by a simple hydrothermal route followed by carbon coating. The effects of the carbon coating on the nanobelts are investigated by Raman spectroscopy, X-ray diffraction (XRD), scanning electron microscope (SEM) with an energy dispersive spectrometer (EDS), a transmission electron microscope (TEM), and galvanostatic cycling. As observed from the TEM and SEM images, the C–MoO_3 nanobelts have a diameter of 150 nm and a length of 5–8 μm. In the electrochemical results, the C–MoO_3 nanobelts exhibit excellent cycling stability after being cycled at a current rate of 0.1 C, maintaining their capacity at 1064 mAh g^{-1} after 50 cycles. These results are better than those for a bare MoO_3 nanobelt electrode. The excellent electrochemical performance of the C–MoO_3 nanobelts can be attributed to the effects of the carbon coating which stabilizes the structure of the MoO_3, enhances the ionic/electrical conductivity, and moreover, can serve as a buffering agent to absorb the volume expansion during the Li^+ intercalation process.

1. Introduction

Lithium-ion batteries (LIBs) are one of the most important types of power source for various existing and potential applications, that include popular mobile devices and next generation electric and hybrid-electric vehicles (EVs/HEVs) because of their high specific energy [1–3]. One of the real challenges in battery design is to ensure that the electrodes maintain their integrity, as this will give the batteries excellent capacity retention and long cycle-life.

Because the electrochemical insertion of lithium into MoO_3 is reversible, the application of this material in LIBs has been widely studied [4]. As an anode material, MoO_3 not only has a superior theoretical specific capacity of nearly 1111 mAh g^{-1} [5], which is more than three times the theoretical capacity of graphite [6], but also has a very stable one-dimensional (1D) layered structure [7,8]. This layered structure is able to act as a temporary support for intercalated species, such as protons, solvated lithium and sodium ions, as well as larger molecules [9]. On the other hand, MoO_3 has poor ionic and electronic conductivity [10], which limits its electrochemical performance. Many researchers have tried to overcome this drawback by doping MoO_3 with Na and Sn [10,11], modifying its structure [12,13], and incorporating it into composites [14]. Among the doped systems, Na-doped MoO_3 shows an initial capacity close to the theoretical value, and such systems are stable after applying a slow rate of current density and increasing the cut-off voltage during cycling up to 100 cycles. With respect to modification of the structure, MoO_3 nanoparticles display excellent performance in terms of durable reversible capacity and high-rate capability. The reversible capacity remains constant up to 150 cycles, and the batteries can be cycled at a current rate as high as 2 C, which possibly meets the requirements for HEV applications. Similar behaviour is also observed with composite compounds; the reversible capacity remains stable without any deterioration during cycling of the electrodes.

In this work, the synthesis of carbon-coated MoO_3 nanobelts and their electrochemical performance as anode composite materials for LIBs are investigated. From a survey of the literature, this is the first report on C–MoO_3 composite nanobelts. The lithium-ion insertion/extraction behaviour of the C–MoO_3 is systematically studied. The capacity of the C–MoO_3 increases with charge–discharge cycling and suggests that the C–MoO_3 nanobelts can be promising anode materials for lithium-ion batteries.

2. Experimental

2.1. Synthesis of materials

Ammonium heptamolybdate tetrahydrate (AHM; $(NH_4)_6Mo_7O_{24}{\cdot}4H_2O$, 99.5%) and nitric acid (HNO_3, 69%) were used as starting reagents to obtain the MoO_3 nanobelts. An amount of 3.12 g or

* Corresponding author at: Institute for Superconducting and Electronic Materials, University of Wollongong, NSW 2522, Australia. Tel.: +61 42981416; fax: +61 42215731.
E-mail address: mfh125@uow.edu.au (M.F. Hassan).

0378-7753/$ – see front matter © 2009 Elsevier B.V. All rights reserved.
doi:10.1016/j.jpowsour.2009.10.065

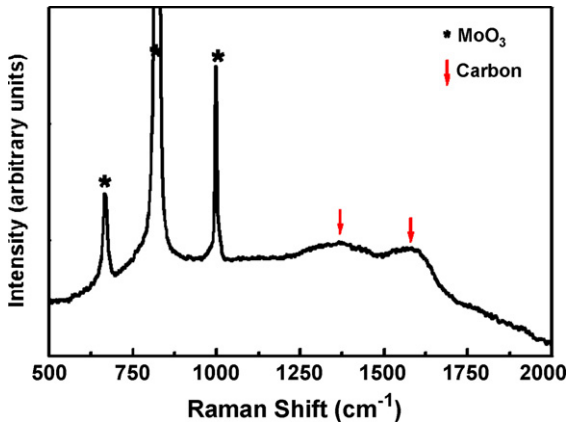

Fig. 1. Raman spectrum of C–MoO_3 composite nanobelt electrode.

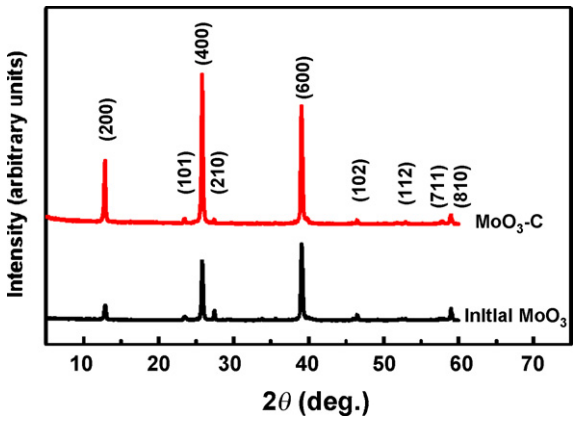

Fig. 2. X-ray diffraction patterns of (a) MoO_3 nanobelts and (b) C–MoO_3 composite nanobelts.

2.5 mmol of the AHM was dissolved in 10 mL distilled water, and then the pH value of the solution was adjusted by using 5 M nitric acid to achieve a pH 1. The resultant solution, together with some white precipitate, was transferred to a Teflon-lined stainless-steel autoclave and maintained at 180 °C for 30 h. The MoO_3 precipitate was filtered and rinsed with a large amount of deionized water, followed by drying at 100 °C for 24 h under a pressure of 10^5 Pa. The MoO_3 nanobelts thus obtained were then coated with carbon. Malic acid (MA) ($C_4H_6O_5$, 99%) was used as the carbon source. The MA was first dispersed in toluene (C_7H_8, 99.5%), and the MoO_3 nanobelts obtained from the hydrothermal technique were added to toluene while stirring at room temperature for 2 h. The slurry was dried at 180 °C for 6 h under a vacuum pressure of 10^5 Pa and given a further heat-treatment at 265 °C for 3 h in an air atmosphere.

2.2. Characterization of bare MoO_3 and C–MoO_3 composite nanobelts

The carbon and MoO_3 compounds were identified by Raman spectroscopy (Jobin Yvon HR800) and X-ray diffraction (XRD; GBC MMA generator), respectively. The morphology of the as-prepared carbon-coated MoO_3 materials was observed by a transmission electron microscope (TEM; JEOL 2011) and a scanning electron microscope (SEM; JEOL JSM 6460A) equipped with energy dispersive spectroscopy (EDS) and an EDS X-ray (EDS-X) mapping system.

2.3. Electrochemical measurements

The anode electrodes were prepared by dispersing 60 wt.% active materials, 20 wt.% carbon black and 20 wt.% poly(vinylidene fluoride) binder in 1-methyl-2-pyrrolidinone solvent to form a slurry. The resulting slurry was pasted on copper foil and dried in vacuum at 120 °C for 12 h. Cells were fabricated for electrochemical testing and were assembled in an argon-filled glove-box (H_2O, O_2 < 0.1 ppm, Mbraun, Unilab, USA). The electrolyte was 1 M $LiPF_6$ in a mixture of ethylene carbonate and dimethyl carbonate (1:1 by volume, provided by MERCK KgaA, Germany), and the separator was microporous polypropylene film. The cells were galvanostati-

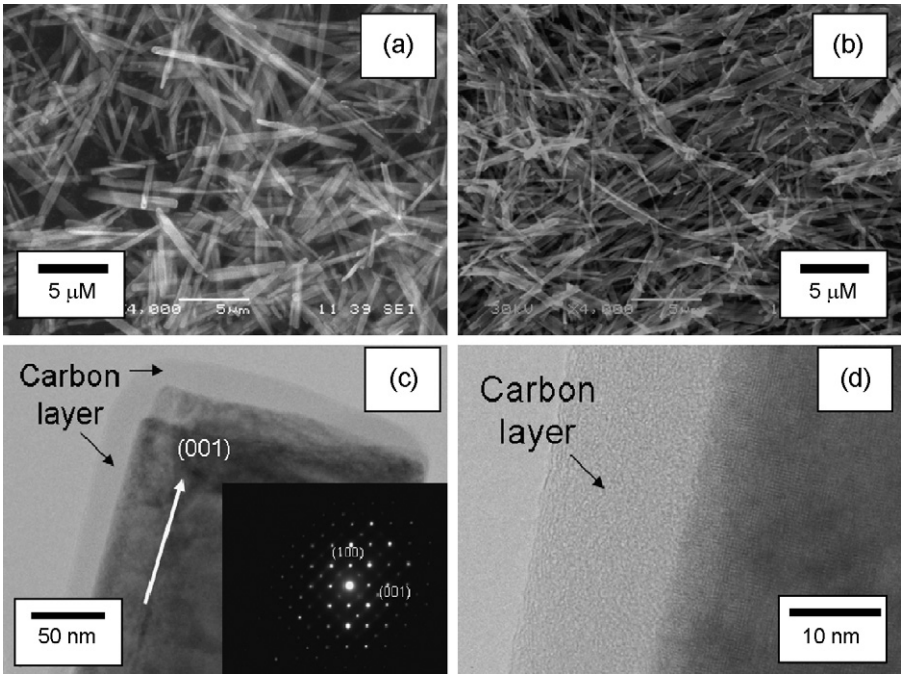

Fig. 3. Scanning electron microscope images of (a) MoO_3 nanobelts and (b) C–MoO_3 composite nanobelts. TEM images of C–MoO_3 composite nanobelts at different magnifications (c) and (d). The inset in (c) shows corresponding SAED pattern.

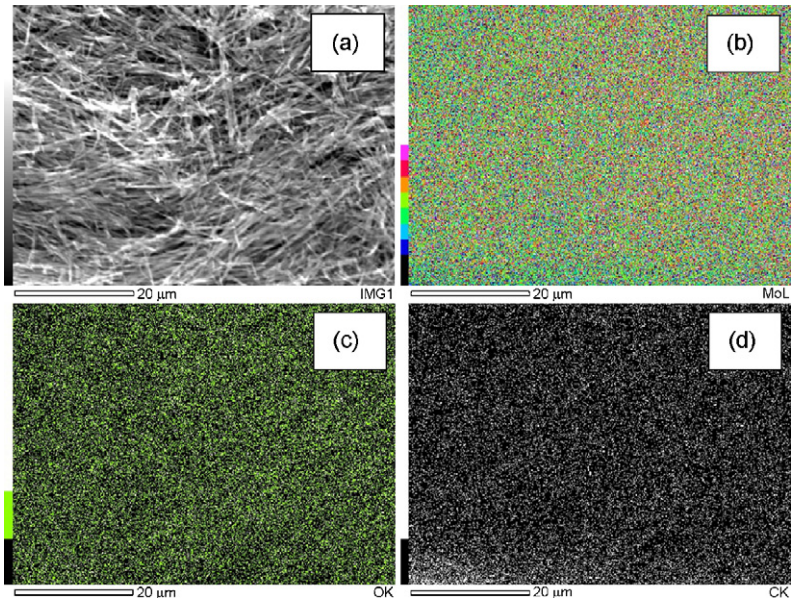

Fig. 4. (a) Scanning electron microscope image of C–MoO_3 composite nanobelts. Corresponding EDS mappings for elements (b) Mo, (c) O, and (d) C.

cally discharged and charged with a Neware battery cycler over a voltage range of 0.05–3.0 V versus Li/Li^+.

3. Results and discussion

3.1. Materials characterization

From previous experience in using MA as the carbon source for carbon coating/deposition on different materials [20], a temperature of 265 °C was chosen for the experiment to decompose the MA and obtain an amorphous carbon layer while minimizing the crystallite growth of the MoO_3. The Raman analysis results confirm the presence of amorphous carbon in the composite nanobelt sample; the spectrum is presented in Fig. 1. A few sharp peaks can be observed, which are located at 671, 825 and 996 cm^{-1}, corresponding to MoO_3 [15,16]. The broad peaks indexed by red arrows at around 1370 and 1580 cm^{-1} are related to amorphous carbon. These peaks are in good agreement with Raman spectra of amorphous carbon reported in the literature [17–19].

X-ray diffraction results show the crystal structures, phases and lattice modification of the bare MoO_3 nanobelts and the C–MoO_3 composite (Fig. 2). All the samples show a number of XRD peaks, positioned at 12.8°, 23.4°, 25.8°, 27.5°, 39.1°, 46.4°, 52.9°, 57.9° and 59.0°, that can be easily indexed as orthorhombic MoO_3 in the Joint Committee on Powder Diffraction Standards (JCPDS) database (JCPDS No. 65-2421, space group: Pnma, no. 62). As can be seen for the C–MoO_3 sample, no carbon peaks can be identified from the XRD pattern. The carbon is hard to trace in XRD analysis due to its amorphous nature and the highly crystalline structure of the MoO_3 nanobelts.

Scanning electron microscope and TEM images of the bare and composite nanobelts are shown in Fig. 3. Several agglomerations of nanobelts can be observed (Fig. 3(a and b)). The nanobelts have an average diameter of around 150 nm and lengths of between 5 and 8 μm. As expected, the C–MoO_3 has a thin layer of amorphous carbon covering the nanobelts, as shown in Fig. 3(c and d). The thickness of the carbon coating is around 15 nm, which is similar to the thickness of carbon coatings on a number of reported composites, such as SnO_2/C, TiO_2/C, and Si/C [20–22]. Such a carbon morphology is expected to improve the ionic/electrical conductivity and the cycling stability of C–MoO_3 electrodes. A TEM image

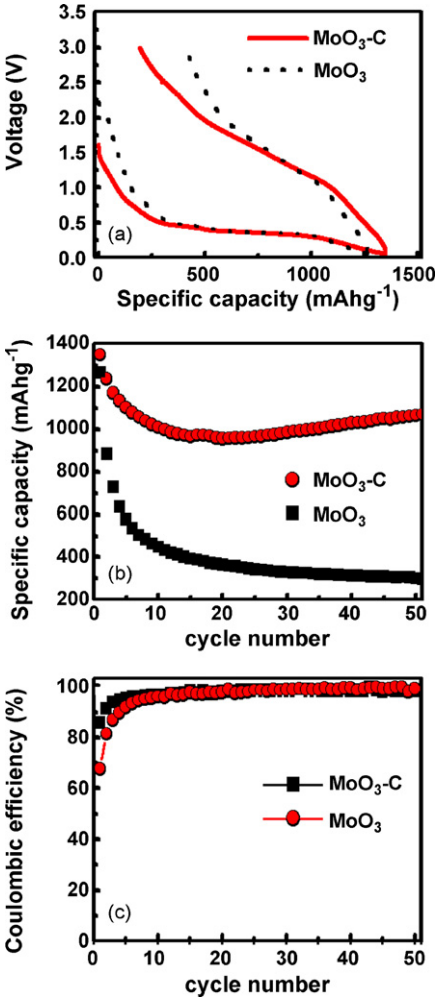

Fig. 5. Voltage profile of (a) first cycle of bare nanobelt and carbon-coated composite nanobelt electrodes; (b) discharge capacity vs. cycle number curves of bare MoO_3 nanobelt and C–MoO_3 composite nanobelt electrodes at current rate of 0.1 C; (c) coulombic efficiency of C–MoO_3 composite nanobelt and bare MoO_3 nanobelt electrodes up to 50th cycle.

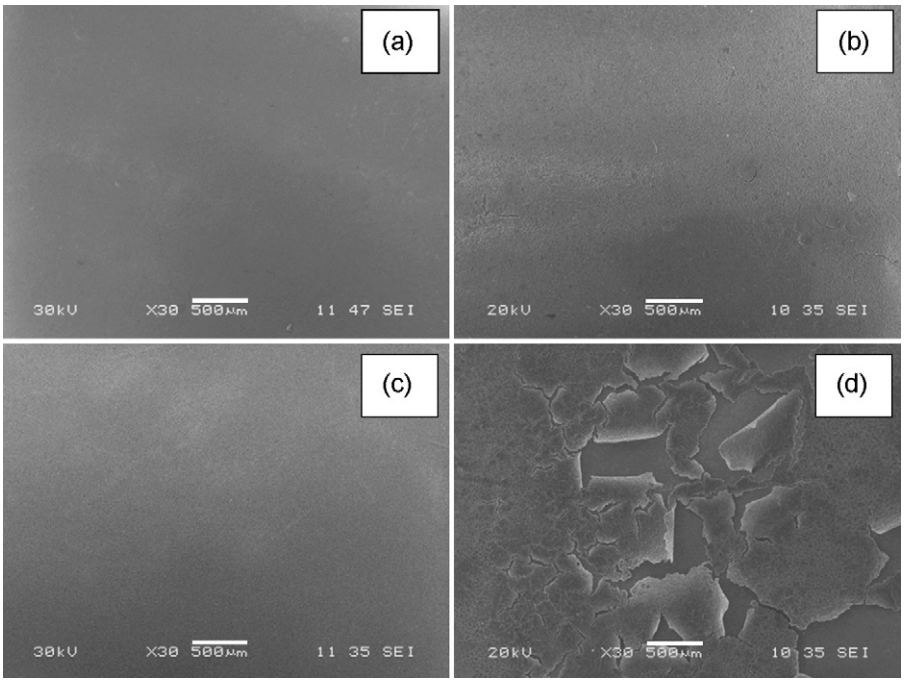

Fig. 6. Scanning electron microscope images at different magnifications of C–MoO_3 composite nanobelts (a) before and (b) after cycling, and bare MoO_3 nanobelts (c) before and (d) after cycling, respectively.

of an individual nanobelt in Fig. 3(c) reveals smooth facets that enclose the surfaces of the nanobelt and form sharp edges, such that the nanobelt has rectangular flat tips with four sharp corners at the ends. The corresponding selected area electron diffraction (SAED) pattern of the nanobelt (inset) can be indexed to the (0 0 1) and (1 0 0) planes. Based on the nanobelt image and its corresponding SAED pattern, it is reasonably clear that the nanobelt has grown along the (0 0 1) crystal direction and terminates at the (0 1 0) and (1 0 0) crystallographic facets (Fig. 3(d)). The EDS results also indicate a uniform carbon distribution, as shown in Fig. 4. Fig. 4(a) is a SEM image of the composite sample, and Fig. 4(b–d) show the corresponding EDS mappings for the elements Mo, O, and C, respectively. The bright spots correspond to the presence of each element. It is obvious that the distribution of carbon in the composite is homogeneous. It is reasonable to conclude that the oxide and carbon particles are thoroughly intermixed.

3.2. Charge–discharge studies on bare MoO_3 and C–MoO_3 composite nanobelt electrodes

The initial charge–discharge curves of the bare nanobelts and the C–MoO_3 composite electrodes are presented in Fig. 5(a), where the composite electrode has an initial irreversible capacity of around 192 mAh g^{-1}, i.e., much smaller than that of bare nanobelts (492 mAh g^{-1}). The initial coulombic efficiency of the bare MoO_3 nanobelts increases from 67.57 to 85.80% after carbon coating (Fig. 5(c)). As discussed in pervious work [20], the improvements in the initial coulombic efficiency and the initial irreversible capacity after carbon coating correlate to elements such as metal atoms and/or oxygen atoms that are not bound to each other on the surface of the metal oxide in the composite, and the presence of the carbon can further enhance the charge transport on the surface of the composite electrode. Fig. 5(b) shows the capacity with cycling at a current rate of 0.1 C from 3.0 to 0.05 V for bare and composite nanobelt electrodes. For the composite nanobelt electrode, the discharge capacity drops in the first 10 cycles; but then gradually increases and reaches 1064 mAh g^{-1} at the 50th cycle. For the bare nanobelt electrode after the first cycle, the discharge capacity drops continuously with cycling, and at the same cycle the discharge capacity remains at about 22.74% of the discharge capacity of the composite sample. The reasons for the outstanding high capacity and capacity retention of the C–MoO_3 composite electrode can be attributed to two factors, namely, the high ionic/electrical conductivity of the carbon-coated sample and the buffering effect of the carbon coating on the MoO_3 nanobelts. It is well-known that such a carbon coating provides electronic conduction channels and facilitates Lithium-ion transport between the active phases, both of which improve the initial coulombic efficiency and enhance the electrochemical properties during lithium insertion and extraction. These improvements are consistent with the results presented in the current study. Lee et al. [12] have found that MoO_3 also experiences a large volume expansion during lithium intercalation into its structure and thereby results in poor capacity retention and cycleability. After carbon coating, however, both capacity retention and cycleability significantly improve, which implies that the carbon coating not only can enhance the electrochemical properties of the compound, but also can effectively buffer the volume expansion and maintain the structural integrity. These improvements can be seen in the SEM images that are presented in Fig. 6(a) (before cycling) and Fig. 6(b) (after cycling). The images show that the composite nanobelt electrode is a tough film, which still adheres strongly to the copper substrate after cycling for over 50 cycles. By contrast, the bare nanobelt electrode displays a continuous loss of capacity with cycling up to 50 cycles; this behaviour is due to damage to the integrity of the nanobelt after charge–discharge cycling and is supported by the SEM images shown in Fig. 6(c) (before cycling) and Fig. 6(d) (after cycling). In summary, the introduction of an amorphous carbon coating on the surfaces of MoO_3 nanobelts can clearly overcome the drawbacks of bare MoO_3 nanobelts to some extent. The carbon coating can not only improve the electrical conductivity of the electrodes but also serve as an effective buffering agent to absorb the volume expansion during Li insertion, thus maintaining the integrity of the electrode. In short, carbon coating can significantly enhance the electrochemical performance of MoO_3 nanobelt electrodes. Carbon-coated MoO_3 composite nanobelts are there-

fore promising anode materials for future lithium-ion batteries, as they exhibit a high charge–discharge capacity and excellent cycling performance.

4. Conclusions

Carbon-coated MoO_3 composite nanobelts have been successfully synthesized via the hydrothermal method followed by carbon coating. Electrochemical measurements demonstrate that the electrode properties of the C–MoO_3 composites are significantly better than those of bare MoO_3 nanobelts. At first, the capacity of the composite nanobelts decreases during cycling over 10 cycles, but then increases gradually and reaches 1064 mAh g^{-1} at the 50th cycle. Compared with bare MoO_3 nanobelts, the composite nanobelts exhibit superior electrochemical performance. The excellent performance may arise from the carbon coating on the nanobelts, which provides good structural stability, increases the electrical conductivity, and acts as a volume buffer to absorb the volume variation during Li^+ insertion.

Acknowledgements

Financial support from the Australian Research Council (ARC) through an ARC Discovery project (377341009) is greatly appreciated. Mohd Faiz Hassan is grateful to the Ministry of Higher Education of the Government of Malaysia for scholarship support. The authors also would like thank Dr. Tania Silver and Dr. T. Seng for critical reading and correction of this manuscript.

References

[1] G. Derrien, J. Hassoun, S. Panero, B. Scrosati, Adv. Mater. 19 (2007) 2336–2340.
[2] H. Uchiyama, E. Hosono, I. Honma, H. Zhou, H. Imai, Electrochem. Commun. 10 (2008) 52–55.
[3] Y. Yu, C.-H. Chen, Y. Shi, Adv. Mater. 19 (2007) 993–997.
[4] M.E. Spahr, P. Novak, O. Haas, R. Nesper, J. Power Sources 54 (1995) 346–351.
[5] H. Li, P. Balaya, J. Maier, J. Electrochem. Soc. 151 (11) (2004) A1878–A1885.
[6] W. Pu, X. He, J. Ren, C. Wan, C. Jiang, Electrochim. Acta 50 (2005) 4140–4145.
[7] H.G. Yang, H.C. Zeng, Angew. Chem. Int. Ed. 43 (2004) 5930–5933.
[8] W. Dong, B. Dunn, J. Non-Cryst. Solids 225 (1998) 135–140.
[9] R. Schollhorn, R. Kuhlmann, J.O. Besenhard, Mater. Res. Bull. 11 (1976) 83–90.
[10] F. Leroux, L.F. Nazar, Solid State Ionics 133 (2000) 37–50.
[11] F. Leroux, G.R. Goward, W.P. Power, L.N. Nazar, Electrochem. Solid-State Lett. 1 (6) (1998) 255–258.
[12] S.-H. Lee, Y.-H. Kim, R. Deshpande, P.A. Parilla, E. Whiteney, D.T. Gillaspie, K.M. Jones, A.H. Mahan, S. Zhang, A.C. Dillon, Adv. Mater. 20 (2008) 3627–3632.
[13] S.-H. Lee, R. Deshpande, D. Benhammou, P.A. Parilla, A.H. Mahan, A.C. Dillon, Thin Solid Films 517 (2009) 3591–3595.
[14] L.C. Yang, Q.S. Gao, Y. Tang, Y.P. Wu, R. Holze, J. Power Sources 179 (2008) 357–360.
[15] L. Mai, B. Hu, W. Chen, Y. Qi, C. Lao, R. Yang, Y. Dai, Z.L. Wang, Adv. Mater. 19 (2007) 3712–3716.
[16] S.-H. Lee, M.J. Seong, C.E. Tracy, A. Mascarenhas, J.R. Pitts, S.K. Deb, Solid State Ionics 147 (2002) 129–133.
[17] J.D. Pasteris, B. Wopenka, Astrobiology 3 (2003) 727–738.
[18] C.J. Yang, J.L. Jiang, D.J. Ping, Z.H. Fei, Chin. Phys. Lett. 25 (2008) 780–782.
[19] A. Guedes, N. Ribeiro, M. Oliveira, F. Noronha, I. Abreu, J. Aerosol Sci. 40 (2009) 81–86.
[20] M.-S. Park, Y.-M. Kang, J.-H. Kim, G.-X. Wang, S.-X. Dou, H.-K. Liu, Carbon 46 (2008) 35–40.
[21] L.J. Fu, H. Liu, H.P. Zhang, C. Li, T. Zhang, Y.P. Wu, R. Holze, H.Q. Wu, Electrochem. Commun. 8 (2006) 1–4.
[22] T. Zhang, L.J. Fu, J. Gao, L.C. Yang, Y.P. Wu, H.Q. Wu, Pure Appl. Chem. 78 (2006) 1889–1896.